Article

A Unified Perspective on the Hydrogen Atom Transfer and Proton-Coupled Electron Transfer Mechanisms in Terms of Topographic Features of the Ground and Excited Potential Energy Surfaces As Exemplified by the Reaction between Phenol and Radicals

Oksana Tishchenko, Donald G. Truhlar, Arnout Ceulemans, and Minh Tho Nguyen

J. Am. Chem. Soc., **2008**, 130 (22), 7000-7010 • DOI: 10.1021/ja7102907 • Publication Date (Web): 09 May 2008

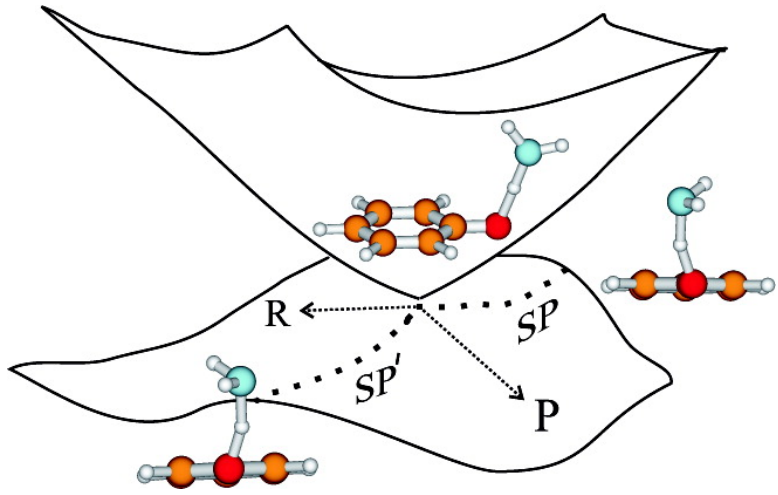

More About This Article

Additional resources and features associated with this article are available within the HTML version:

- Supporting Information
- Links to the 3 articles that cite this article, as of the time of this article download
- Access to high resolution figures
- Links to articles and content related to this article
- Copyright permission to reproduce figures and/or text from this article

View the Full Text HTML

J|A|C|S
ARTICLES

Published on Web 05/09/2008

A Unified Perspective on the Hydrogen Atom Transfer and Proton-Coupled Electron Transfer Mechanisms in Terms of Topographic Features of the Ground and Excited Potential Energy Surfaces As Exemplified by the Reaction between Phenol and Radicals

Oksana Tishchenko,*,†,‡ Donald G. Truhlar,*,† Arnout Ceulemans,‡ and Minh Tho Nguyen‡

Department of Chemistry and Supercomputing Institute, University of Minnesota, Minneapolis, Minnesota 55455-0431, and Department of Chemistry and Mathematical Modelling and Computational Science Center, University of Leuven, B-3001 Leuven, Belgium

Received November 13, 2007; E-mail: o_t@t1.chem.umn.edu; truhlar@umn.edu

Abstract: The relation between the hydrogen atom transfer (HAT) and proton-coupled electron transfer (PCET) mechanisms is discussed and is illustrated by multiconfigurational electronic structure calculations on the ArOH + R$^\bullet$ → ArO$^\bullet$ + RH reactions. The key topographic features of the Born–Oppenheimer potential energy surfaces that determine the predominant reaction mechanism are the conical intersection seam of the two lowest states and reaction saddle points located on the shoulders of this seam. The saddle point corresponds to a crossing of two interacting valence bond states corresponding to the reactant and product bonding patterns, and the conical intersection corresponds to the noninteracting intersection of the same two diabatic states. The locations of mechanistically relevant conical intersection structures and relevant saddle point structures are presented for the reactions between phenol and the N- and O-centered radicals, $^\bullet NH_2$ and $^\bullet OOCH_3$. Points on the conical intersection of the ground doublet D_0 and first excited doublet D_1 states are found to be in close geometric and energetic proximity to the reaction saddle points. In such systems, either the HAT mechanism or both the HAT mechanism and the proton-coupled electron transfer (PCET) mechanism can take place, depending on the relative energetic accessibility of the reaction saddle points and the D_0/D_1 conical intersection seams. The discussion shows how the two mechanisms are related and how they blend into each other along intermediate reaction paths. The recognition that the saddle point governing the HAT mechanism is on the shoulder of the conical intersection governing the PCET mechanism is used to provide a unified view of the competition between the two mechanisms (and the blending of the two mechanisms) in terms of the prominent and connected features of the potential energy surface, namely the saddle point and the conical intersection. The character of the dual mechanism may be understood in terms of the dominant valence bond configurations of the intersecting states, which are zero-order approximations to the diabatic states.

1. Introduction

The mechanistic distinction between hydrogen atom transfer (HAT) and proton-coupled electron transfer (PCET) is crucial to understanding the effects of changing reaction variables such as structure and environment (solvent, enzyme, or other catalyst) on reactivity in systems that can exhibit both mechanisms. Thus, such systems present both the challenge and the opportunity to clarify the issues involved in this distinction. Experiments[1] on reactions of phenols with free radicals that involve the abstraction of the hydroxylic hydrogen

$$R^\bullet + ArOH \rightarrow ArO^\bullet + RH \qquad (1)$$

show that, depending on the reactants and the environment, these reactions can proceed via at least three different mechanisms:[1] (i) HAT, (ii) PCET, and (iii) the recently proposed[1,2] sequential proton-loss electron transfer (SPLET) route. Both the HAT and PCET mechanisms involve a single reaction step (no reaction intermediates) and thus can be considered as a "single-event electron transfer with atom transfer",[3] although when R$^\bullet$ has an unshared pair of electrons, reaction 1 is preceded by the formation of an ArOH···R$^\bullet$ hydrogen-bonded complex[4] in both HAT and PCET mechanisms. Various criteria can be used to distinguish between HAT and PCET; the criterion we use is electronic adiabaticity or nonadiabaticity. The HAT reaction is electronically adiabatic, whereas the transfer of a proton and an electron in the PCET reaction involves electronic nonadia-

† University of Minnesota.
‡ University of Leuven.

(1) For a recent review, see: Litwinenko, G.; Ingold, K. U. *Acc. Chem. Res.* **2007**, *40*, 222.
(2) Litwinenko, G.; Ingold, K. U. *J. Org. Chem.* **2004**, *69*, 5888.
(3) Cannon, R. D. *Electron Transfer Reactions*; Butterworths: 1980; p 29.
(4) Ahrens, B.; Davidson, M. G.; Forsyth, V. T.; Mahon, M. F.; Johnson, A. L.; Mason, S. A.; Price, R. D.; Raithby, P. R. *J. Am. Chem. Soc.* **2001**, *123*, 9164.

10.1021/ja7102907 CCC: $40.75

batic effects.[5] Both mechanisms are net electronically adiabatic in that they proceed from ground-electronic state reactants to ground-electronic state products, but PCET will be locally electronically nonadiabatic in the critical region. The nonadiabaticity is promoted by an intersection or strong interaction of two or more potential energy surfaces. (This criterion for distinguishing HAT from PCET will be compared to other criteria in section 3.) Both the HAT and PCET mechanisms are contrasted to the stepwise SPLET mechanism, which involves more than one kinetic reaction step.[2] The relationship between the HAT and PCET mechanisms is critical for understanding a wide variety[5–21] of reactions; we will consider reaction 1 as an example to elucidate broadly applicable concepts.

The present article will illustrate the potential energy surface features of systems of the type of reaction 1 that govern both the HAT mechanism and the PCET mechanism by applying ab initio electronic structure calculations to a few of the lowest electronic states of prototype reactive systems, in particular, reactions between the phenol molecule and the $^{\bullet}OOCH_3$ and $^{\bullet}NH_2$ radicals. This class of reactions is important not only as a field on which alternative mechanisms compete but also as a class of reactions that is important in a variety of biological processes. Examples involve the formation of tyrosine phenoxyl radicals (tyrosyl radicals) in proteins and enzymes[22] and the functioning of natural phenolic antioxidants, such as tocopherol (Vitamin E).[23] The phenoxyl radical is also important in combustion.[24]

The remaining parts of this paper are organized as follows. Section 2 summarizes computational methods, Section 3 presents the results for geometries and energetics of the critical points of the $ArOH\cdots NH_2$ and $ArOH\cdots OOCH_3$ systems (focusing only on the points most important for subsequent discussion, where the systems serve as examples) followed by discussion focusing on orbitals, implications for mechanisms and dynamics, mechanistic distinctions in terms of the topographic features of potential energy surfaces, and relationships to other viewpoints. Section 4 contains summarizing remarks.

2. Computational Methods

We will present calculations on the reaction of phenol with $^{\bullet}NH_2$ and $^{\bullet}OOCH_3$ radicals to illustrate the concepts. We use multireference methods with large active spaces but moderate one-electron basis sets; this is adequate for the present work where we are more interested in rationalizing the shape of the ground-state PES than in achieving chemical accuracy for the reaction barrier heights. Here we summarize the methods at a level sufficient for introducing the subsequent discussion; additional details of the electronic structure calculations are given in the Supporting Information.

Orbitals and critical geometries on the ground-state potential energy surface were optimized by using multiconfigurational self-consistent field wave functions of the fully optimized reaction space (FORS[25a]) type (equivalent to single-state complete-active-space-self-consistent field, CASSCF[25b,c]). Calculations that include more than one electronic state are based on state-averaged CASSCF (SA-CASSCF) wave functions where the three ($R^{\bullet} = {}^{\bullet}NH_2$) or two ($R^{\bullet} = {}^{\bullet}OOCH_3$) lowest electronically adiabatic states are included with equal weights (the three lowest electronically adiabatic states are called D_0, D_1, and D_2 as usual). All active spaces used in the present work are described in detail in the Supporting Information. Dynamical electron correlation was included by using multireference second-order Møller–Plesset theory (MRMP2)[26] and multiconfiguration quasi-degenerate perturbation theory MCQDPT.[27] All calculations are performed using the GAMESS[28] and MOLPRO[29] suites of programs.

3. Results and Discussion

Selected geometrical parameters of the hydrogen-bonded precursor ($ArOH\cdots R$) and successor ($ArO\cdots HR$) complexes and geometries of the saddle point (SP) structures are given in Tables 1 and 2 with the labeling of Figure 1; the complete list of geometrical parameters of optimized structures is available in the Supporting Information.

Hydrogen-Bonded Precursor Complexes. The isolated phenol molecule in its ground electronic state is known to possess a 2-fold torsional barrier[30] for the internal rotation of the OH group with minima at the two equivalent planar structures. The corresponding two equilibrium structures for the $ArOH\cdots R$

(5) (a) See e.g.; Hammes-Schiffer, S. *Acc. Chem. Res.* **2001**, *34*, 273. (b) Mayer, J. M. *Annu. Rev. Phys. Chem.* **2004**, *55*, 363.
(6) Cukier, R.; Nocera, D. G. *Annu. Rev. Phys. Chem.* **1998**, *49*, 337.
(7) Roth, J. P.; Lovell, S.; Mayer, J. M. *J. Am. Chem. Soc.* **2000**, *122*, 5486.
(8) Luzhkov, V. B. *Chem. Phys.* **2005**, *314*, 211.
(9) Costentin, C.; Evans, D. H.; Robert, M.; Saveat, J.-M.; Singh, P. S. *J. Am. Chem. Soc.* **2005**, *127*, 12490.
(10) Yuasa, J.; Fukuzumi, S. *J. Am. Chem. Soc.* **2006**, *128*, 14281.
(11) Skone, J. H.; Soudackov, A. V.; Hammes-Schiffer, S. J. *Am. Chem. Soc.* **2006**, *128*, 16655.
(12) Hodgkiss, J. M.; Rosenthal, J.; Nocera, D. G. In *Hydrogen Transfer Reactions*; Hynes, J. T., Klinman, J. P., Limbach, H. H., Schowen, R. L., Eds.; Wiley-VCH: Weinheim, 2007; Vol. 2, p 503.
(13) Reece, S. Y.; Hodgkiss, J. M.; Stubbe, J.; Nocera, D. G. *Phil. Trans. R. Soc. London, Ser. B* **2006**, *361*, 1351.
(14) Rhile, I. J.; Markle, T. F.; Nagao, H.; DiPasquale, A. G.; Lam, O. P.; Lockwood, M. A.; Rotter, K.; Mayer, J. M. *J. Am. Chem. Soc.* **2006**, *128*, 6075.
(15) Mader, E. A.; Davidson, E. R.; Mayer, J. M. *J. Am. Chem. Soc.* **2007**, *129*, 5153.
(16) DiLabio, G. A.; Johnson, E. R. *J. Am. Chem. Soc.* **2007**, *129*, 6199.
(17) Chen, X.; Bu, Y. *J. Am. Chem. Soc.* **2007**, *129*, 9713.
(18) DiLabio, G. A.; Ingold, K. U. *J. Am. Chem. Soc.* **2005**, *127*, 6693.
(19) Mayer, J. M.; Hrovat, D. A.; Thomas, J. L.; Borden, W. T. *J. Am. Chem. Soc.* **2002**, *124*, 11142.
(20) Costentin, C.; Robert, M.; Saveat, J.-M. *J. Am. Chem. Soc.* **2007**, *129*, 9953.
(21) Ishikita, H.; Soudackov, A. V.; Hammes-Schiffer, S. *J. Am. Chem. Soc.* **2007**, *129*, 11146.
(22) (a) Sjödin, M.; Styring, S.; Åkermark, B.; Sun, L.; Hammarström, L. *J. Am. Chem. Soc.* **2000**, *122*, 3932. (b) Siegbahn, P. E. M.; Eriksson, L.; Himo, F.; Pavlov, M. *J. Phys. Chem. B* **1998**, *102*, 10622. (c) Lundqvist, M. J.; Eriksson, L. A. *J. Phys. Chem. B* **2000**, *104*, 848. (d) O'Malley, P. J. *J. Am. Chem. Soc.* **1998**, *120*, 11732. (e) Maki, T.; Araki, Y.; Ishida, Y.; Onomura, O.; Matsumura, Y. *J. Am. Chem. Soc.* **2001**, *123*, 3371. and references therein.
(23) (a) Burton, G. W.; Ingold, K. U. *Acc. Chem. Res.* **1986**, *19*, 194. (b) Niki, E. *Chem. Phys. Lipids* **1987**, *44*, 227. (c) Niki, E.; Noguchi, N. *Acc. Chem. Res.* **2004**, *37*, 45.
(24) (a) Lin, C.-Y.; Lin, M. C. *J. Phys. Chem.* **1986**, *90*, 425. (b) *Soot Formation in Combustion - Mechanisms and Models*; Bockhorn, H., Ed.; Springer-Verlag: New York, 1993. (c) Horn, C.; Roy, K.; Frank, P.; Just, T. *Proc. Int. Symp. Combustion* **1998**, *27*, 321. (d) Ledesma, E. B.; Nelson, P. F.; Mackie, J. C. *Proc. Int. Symp. Combustion* **2000**, *28*, 2345. (e) Ross, A. B.; Jones, J. M.; Chaiklangmuang, S.; Pourkashanian, M.; Williams, A.; Kubica, K.; Andersson, J. T.; Kerst, M.; Danihelka, P.; Bartie, K. D. *Fuel* **2002**, *81*, 571.
(25) (a) Ruedenberg, K.; Schmidt, M. W.; Gilbert, M. M.; Elbert, S. T. *Chem. Phys.* **1982**, *71*, 41. (b) Roos, B. O.; Taylor, P. *Chem. Phys.* **1980**, *48*, 157. (c) Werner, H.-J.; Knowles, P. J. J. *Chem. Phys.* **1985**, *82*, 5053.
(26) (a) Hirao, K. *Chem. Phys. Lett.* **1992**, *190*, 374. (b) Hirao, K. *Chem. Phys. Lett.* **1992**, *196*, 397. (c) Hirao, K. *Chem. Phys. Lett.* **1993**, *201*, 59. (d) Hirao, K. *Int. J. Quantum Chem.* **1992**, *26*, 517.
(27) Nakano, H. J. *Chem. Phys.* **1993**, *99*, 7983.
(28) Schmidt, M. W.; Baldridge, K. K.; Boatz, J. A.; Elbert, S. T.; Gordon, M. S.; Jensen, J. H.; Koseki, S.; Matsunaga, N.; Nguyen, K. A.; Su, S. J.; Windus, T. L.; Dupuis, M.; Montgomery, J. A. *J. Comput. Chem.* **1993**, *14*, 1347.
(29) MOLPRO is a package of ab initio programs designed by Werner, H.-J.; Knowles, P. J. version 2002.1, Amos, R. D. et al.

Table 1. Selected Geometrical Parameters for Key Structures of the Hydrogen Abstraction in the Phenol−R System (R = NH_2)[a]

	ArOH···R	SP	MECP	ArO···HR
distance, O_7 N_8	3.108	2.428	2.473	3.399
distance, O_7 H_{14}	0.966	1.197	1.258	2.457
distance, N_8 H_{14}	2.150	1.255	1.215	1.021
distance, C_5 O_7	1.352	1.340	1.310	1.237
angle, N_8 H_{14} O_7	171.4	163.4	179.4	153.1
angle, H_{16} N_8 H_{15}	105.6	105.3	116.8	107.2
dihedral, (H_{14} O_7 C_5 C_4)	0.3	−106.0	−89.7	0.0
dihedral, (N_8 O_7 C_5 C_4)	−0.2	−97.3	−89.6	0.0

[a] Hydrogen-bonded complexes and the saddle point are optimized by FORS(9/9), and the minimum-energy crossing point (MECP) of the D_0 and D_1 states is located using SA-CASSCF(11/10). See Figure 1 for the definition of geometrical parameters. Bond lengths are in Å; bond angles are in degrees.

Table 2. Selected Geometrical Parameters for Key Structures of the Hydrogen Abstraction in the Phenol−R System (R = $OOCH_3$)[a]

	ArOH···R	SP	ArO···HR
distance, O_7 O_8	3.250	2.382	3.020
distance, O_7 H_{14}	0.963	1.158	2.059
distance, O_8 H_{14}	2.295	1.230	0.970
distance, C_6 O_7	1.356	1.322	1.237
angle, O_7 H_{14} O_8	171.1	171.7	170.3
dihedral, (H_{14} O_7 C_6 C_1)	0.0	−79.6	7.7
dihedral, (O_8 O_7 C_6C_1)	0.0	−81.5	7.2

[a] See Figure 1 for the definition of geometrical parameters. Bond lengths are in Å; bond angles are in degrees.

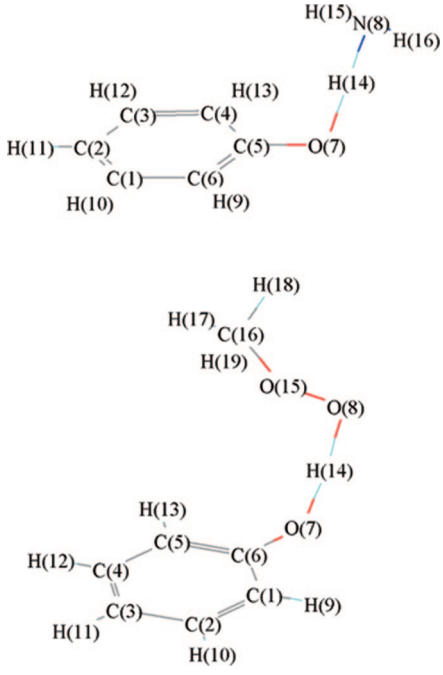

Figure 1. Atomic numbering in the ArOH···NH_2 and ArOH···$OOCH_3$ systems.

complexes are characterized by C_s symmetry, with the OH bond, the hydrogen bond, and the ring plane in the symmetry plane. In the case of ArOH···NH_2, the ground electronic state is $^2A'$ with the nitrogen lone pair that is involved in the hydrogen bond and the nitrogen SOMO that is orthogonal to it both lying in the ring plane, as shown schematically in Figure 2 (left). In the case of ArOH···$OOCH_3$, the ground electronic state is $^2A''$ with the free radical's lone pair that is involved in the hydrogen bond being centered in the ring plane and with the π-type SOMO of

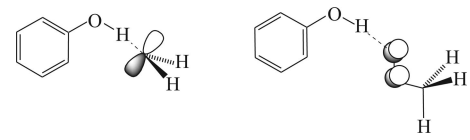

Figure 2. Orientation of the SOMO in ArOH···R precursor complexes.

$^{\bullet}OOCH_3$ orthogonal to this plane (Figure 2, right). The equilibrium geometries of the ArO···HNH_2 and ArO···$HOOCH_3$ complexes in their electronic ground state are both similarly characterized by the coplanarity of the hydrogen bonds with the ring plane. The electronic ground state of these species is $^2A''$ with a π symmetry SOMO delocalized over the phenoxyl oxygen atom and ring.

Saddle Points. While coplanar with the ring plane in the energy-minimum structures, the H-bond becomes twisted out of the ring plane in both SP structures (see Tables 1 and 2). This structural change is promoted by better orbital overlap between the free radical SOMO and the incipient phenoxyl radical π-type SOMO, and hence the ground A″ state of the product ArO radical is stabilized by electron delocalization over the π-electron system (see also ref 31). The zero-point-exclusive reaction barriers (i.e., classical barrier heights) calculated as differences between the Born–Oppenheimer potential energies at the optimized geometries of the ArOH···R complexes and the corresponding H-transfer saddle points at the MRMP2/6-31+G(d,p)//FORS(9/9)/6-31G(d,p) level are 8.1 kcal/mol for R$^{\bullet}$ = $^{\bullet}NH_2$ and 12.5 kcal/mol for R$^{\bullet}$ = $^{\bullet}OOCH_3$.

***D_0/D_1* Conical Intersections.** Two electronic configurations, specifically with the unpaired electron placed in either a $p\pi$ orbital of R (as in Figure 2) or in the phenol's delocalized π orbital, play key roles in the electronic rearrangement process in reaction 1. The electronic structure may be conveniently discussed in terms of diabatic states,[32] that is, electronic configurations with slowly varying character that do not diagonalize the electronic Hamiltonian. In such a description, in the reactant region of ArOH···R, the D_0 state is dominated by the diabatic state Ψ_1 with the unpaired electron mainly in the 2p orbital of R, and the D_1 state is dominated by the diabatic state Ψ_2 with the unpaired electron mainly in the phenol's $p\pi_O$ orbital which is partly delocalized over the phenoxyl ring. In the product region, the D_0 and D_1 states switch their dominant characters. At intermediate geometries the D_0 and D_1 states exhibit a conical intersection along a multidimensional seam (this seam or hypersurface is expected[33] to have dimensionality 3N-8, where N is the number of atoms in ArOH···R). At such

(30) (a) The current best estimate of the rotational barrier in phenol is 3.5 kcal/mol. See: Larsen, N. W. *J. Mol. Struct.* **1986**, *144*, 83. (b) Zierkiewicz, W.; Michalska, D.; Hobza, P. *Chem. Phys. Lett.* **2004**, *386*, 95. (c) Zierkiewicz, W.; Michalska, D.; Černý, J. *Hobza Mol. Phys.* **2006**, *104*, 2317.
(31) (a) de Heer, M. I.; Mulder, P.; Korth, H.-G.; Ingold, K. U.; Lusztyk, J. *J. Am. Chem. Soc.* **2000**, *122*, 2355. (b) Tishchenko, O.; Kryachko, E. S.; Nguyen, M. T. *J. Mol. Struct.* **2002**, *615*, 247. (c) Lucarini, M.; Mugnaini, V.; Pedulli, G. F.; Guerra, M. *J. Am. Chem. Soc.* **2003**, *125*, 8318. (d) Sun, Y.-M.; Liu, C.-B. *Eur. J. Org. Chem.* **2004**, 120.
(32) (a) Lichten, W. *Phys. Rev.* **1963**, *131*, 229. (b) O'Malley, T. F. *J. Adv. At. Mol. Phys.* **1971**, *7*, 223. (c) Numrich, R. W.; Truhlar, D. G. *J. Phys. Chem.* **1975**, *79*, 2745. (d) Delos, J. B.; Thorson, W. R. *J. Chem. Phys.* **1979**, *70*, 1774. (e) Spiegelman, F.; Malrieu, J. P. *J. Phys. B* **1984**, *17*, 1259. (f) Sidis, V. *Adv. Chem. Phys.* **1992**, *82*, 187. (g) Pacher, T.; Cederbaum, L. S.; Köppel, H. *Adv. Chem. Phys.* **1993**, *84*, 293. (h) Thürwachter, R.; Halvick, P. *J. Chem. Phys.* **1997**, *221*, 33. (i) Nakamura, H.; Truhlar, D. G. J. *Chem. Phys.* **2002**, *117*, 5576. (j) Truhlar, D. G. *J. Comput. Chem.* **2007**, *28*, 73.

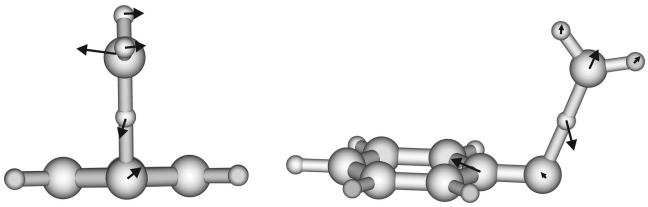

Figure 3. Distortional modes corresponding to the derivative coupling (right) and the gradient difference (left) vectors at the MECP in the $PhOH\cdots NH_2$ system.

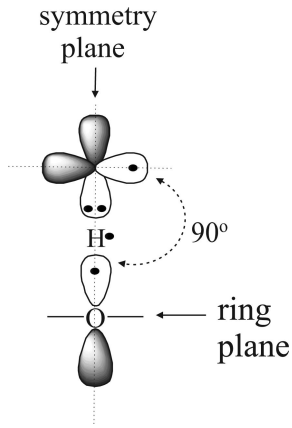

Figure 4. Orientation of the two possible singly occupied MOs in the case where the intersection is allowed by symmetry. A lone pair on the free radical center which is involved in the H-bonding is also shown.

an intersection the nonadiabatic coupling is singular (infinite), and trajectories or wave packets that pass close to such an intersection will not be electronically adiabatic.[33,34]

Geometrical parameters of the minimum energy crossing point (MECP), i.e., the minimum on the D_0/D_1 conical intersection seam, in the $ArOH\cdots NH_2$ system are listed in Table 1. In contrast to the SP, the O···H···R nuclear arrangement is nearly collinear at this structure. Figure 3 displays the directions of the gradient difference vector and the derivative coupling vector that form the branching plane[35] for the D_0/D_1 conical intersection in the $ArOH-NH_2$ system. The derivative coupling vector corresponds to a motion of the hydrogen between two heavy atoms coupled with the C−O stretching motion. The gradient difference vector is dominated by an angular distortion coordinate that changes the orbital hybridization at the nitrogen center from sp^2 at the MECP to sp^3 at the SP. It corresponds to a motion from the apex of the cone toward transition state structures $ArO\cdots H\cdots NH_2$ (there are two isoenergetic $ArO\cdots H\cdots NH_2$ saddle point structures on the "left" and "right" side of the conical intersection at the MECP geometry).

A case for which the D_0/D_1 intersection can be understood by symmetry considerations is illustrated schematically in Figure 4. If the singly occupied atomic orbital on the free radical remains orthogonal to the delocalized phenoxyl portion of the SOMO on the phenoxyl radical along the hydrogen transfer

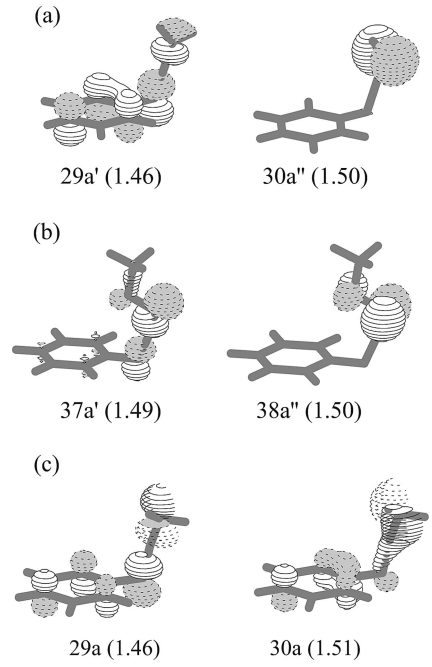

Figure 5. Shapes of the two key MOs of the $ArOH\cdots NH_2$ system (a) and of the $ArOH\cdots OOCH_3$ system (b) (SA-CASSCF(11/10) natural orbital sets) at a geometry similar to the saddle point but that has a symmetry plane. Panel (c) shows the corresponding orbitals of the $ArOH\cdots NH_2$ system at the SP geometry. Numbers in parentheses indicate state-averaged electron occupancies in the D_0 and D_1 states.

coordinate, the two lowest states exhibit a conical intersection for geometries with C_s symmetry. This condition is satisfied for both reactions considered here when the hydrogen transfer coordinate is in the symmetry plane perpendicular to the ring plane. Two key molecular orbitals in this situation are shown in the first two panels of Figure 5. In the case of $R = {}^{\bullet}NH_2$, the molecular orbitals that generate the two dominant configurations are 29a′ and 30a″, and in the case of $R = {}^{\bullet}OOCH_3$, these orbitals are 37a′ and 38a″. Near the SP, at a geometry that does not have a plane of symmetry, both the D_0 and D_1 states in the $ArO\cdots NH_2$ system represent a mixture of these two configurations, in particular $(29a)^2(30a)^1$ and $(29a)^1(30a)^2$, with nearly equal weights. The unpaired electron is delocalized over the 29a and 30a molecular orbitals which are shown for the SP geometry in panel (c) of Figure 5. These two MOs are formed from the NH_2 radical's SOMO and the delocalized π-symmetry orbital of phenol. The interaction of Ψ_1 with Ψ_2 does not vanish at the SP.

Even in the absence of symmetry, the existence of a conical intersection can be demonstrated using a phase tracking argument based on the fact that the ground-state electronic wave function changes sign along a complete traversal of a closed loop if and only if the loop contains a conical intersection (this feature is reviewed and proved elsewhere[33] and has been invoked in a variety of applications).[36] To apply this here we recall that the SP structure can be reached from the MECP by following the direction of the gradient difference vector. By inverting this vector through the origin, we find the mirror image of the transition state structure, say SP′, in the opposite direction. This is schematically shown in the diagram of Figure 6 (upper panel). We now consider a closed path starting at the reactants, going around the crossing point via SP, through the products and back to the reactants via SP′. The wave function changes are also indicated in the diagram. ψ_a is the singly occupied $2p$-

(33) Jasper, A. W.; Kendrick, B. K.; Mead, C. A.; Truhlar, D. G. In *Modern Trends in Chemical Reaction Dynamics*; Yang, X., Liu, K., Eds.; Advanced Series in Physical Chemistry 14; World Scientific: River Edge, NJ, 2004; pp 329–391. See especially pp 339–344
(34) Teller, E. *J. Phys. Chem.* **1937**, *41*, 109.
(35) (a) Atchity, G. J.; Xantheas, S. S.; Ruedenberg, K. *J. Chem. Phys.* **1991**, *95*, 1862. (b) Yarkony, D. R. *Acc. Chem. Res.* **1998**, *31*, 511.

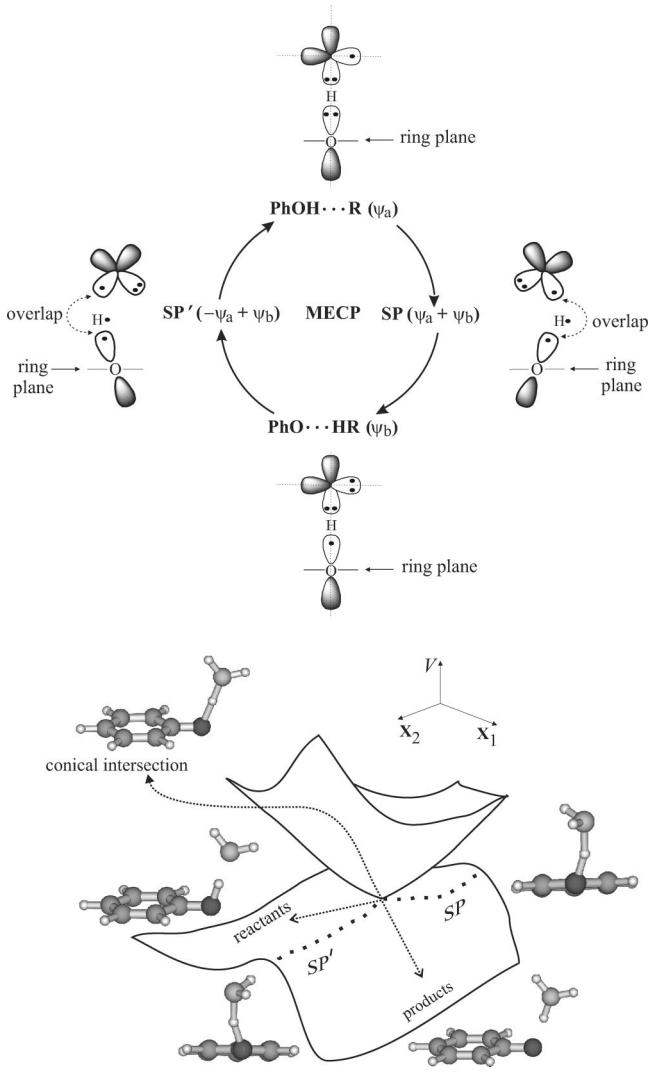

Figure 6. (a) Representation of the geometric phase effect in the ArOH···R system. ψ_a and ψ_b are the singly occupied orbitals in reactants and products, respectively; the H-bonding acceptor orbital (doubly occupied in most configurations) is also shown. (b) Intersecting potential energy surfaces for the situation described by part (a); X_1 and X_2 are the derivative coupling and gradient difference vectors, respectively. A path from reactants to SP to products to SP′ and back to reactants corresponds to the path indicated by arrows on the upper part of this figure. See section 3 for more details.

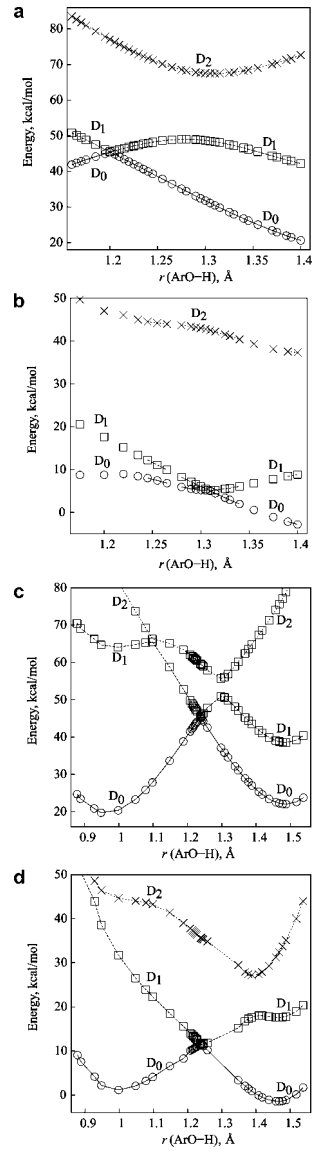

Figure 7. (a) SA-CASSCF(13/11)/6-31+G(d,p) and (b) MCQDPT(13/11)/6-31+G(d,p) sections of the ground D_0 (○) and two excited D_1 and D_2 (□ and ×, respectively) adiabatic PESs of the ArOH···NH_2 system as functions of the H-transfer coordinate for transfer in the symmetry plane perpendicular to the ring plane. In each case, all atoms of the donor and acceptor radicals have their internal coordinates fixed at their values in the SP structure, and the abscissa corresponds to moving the transferring H atom along a straight line from one radical to the other. The zero of energy for each plot is set to the energy of the D_0 state at the precursor complex geometry as calculated with the same level of theory. (c) and (d) are the same as (a) and (b), but they are for transfer in the symmetry plane in the ring plane.

type orbital of the reactant free radical, while ψ_b is the delocalized π orbital of the phenoxyl oxygen and ring; the latter is singly occupied in the product. At SP the ground state involves a linear combination of these two orbitals, schematically represented as $(\psi_a + \psi_b)$. In the mirror image state, SP′, the phase of ψ_a must be changed in this combination due to the nodal structure of the p orbital of ψ_a. The phase tracking argument now states that, starting from $+\psi_a$, under adiabatic changes the wave function will vary smoothly from $(\psi_a + \psi_b)$ to $+\psi_b$ and then to $(-\psi_a + \psi_b)$. In the final quarter of the loop, from SP′ back to reactants, this $(-\psi_a + \psi_b)$ combination will gradually end up in $-\psi_a$. Hence there is a sign change of the wave function over a closed loop, and this indicates that the loop surrounds a conical intersection. The conical intersection is part of a multidimensional seam of intersections of D_0 and D_1. When the symmetry is lowered due to substitution, SP and SP′ need no longer be equivalent, but even in this case the phase tracking argument remains valid, since it is based on the intrinsic nodal characteristics of the orbitals involved in electron transfer.

Figure 7 shows cuts through the lowest doublet state potential energy surfaces along the H-transfer reaction coordinate when

(36) (a) Herzberg, G.; Longuet-Higgins, H. C. *Discuss. Faraday Soc.* **1963**, *35*, 77. (b) Longuet-Higgins, H. C. *Proc. R. Soc. London, Ser. A* **1975**, *344*, 147. (c) Davidson, E. R. *J. Am. Chem. Soc.* **1977**, *99*, 397–402. (d) Mead, C. A.; Truhlar, D. G. *J. Chem. Phys.* **1979**, *70*, 2284. (e) Yarkony, D. R. *J. Chem. Phys.* **1996**, *104*, 7866. (f) Fukumoto, Y.; Koizumi, H.; Makorh, K. *Chem. Phys. Lett.* **1999**, *313*, 283. (g) Zilberg, S.; Haas, Y. *J. Am. Chem. Soc.* **2002**, *124*, 10683. (h) Polinger, V. Z.; Huang, R. W.; Dunn, J. L.; Bates, C. A. *J. Chem. Phys.* **2002**, *117*, 4340. (i) Rozgonyi, T.; Gonzalez, L. *J. Phys. Chem. A* **2006**, *110*, 10251.

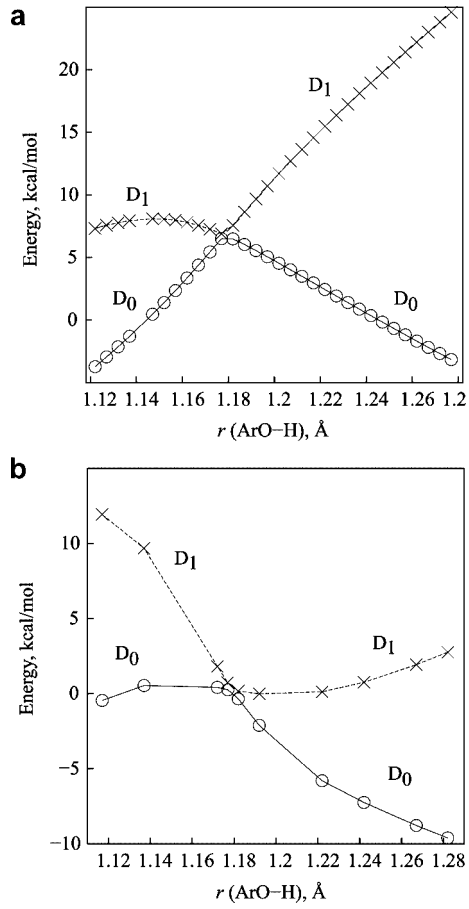

Figure 8. SA-CASSCF(11/10)/6-31+G(d,p) (a) and MCQDPT(11/10)/6-31+G(d,p) (b) sections of the two lowest adiabatic PESs of the ArOH···$OOCH_3$ system as functions of the H-transfer coordinate for transfer in the symmetry plane perpendicular to the ring plane. As in Figure 7, the internal coordinates of the donor and acceptor radicals are fixed at their values in the SP structure. The zero of energy is set to the energy of the D_0 state at the reaction saddle point geometry as calculated with the same level of theory.

the transferring H is moving perpendicular to the ring (parts a and b) or moving in the ring plane (parts c and d). First consider Figure 7a and 7b, which correspond to the orientation shown schematically in Figure 4. At r(OH) distances shorter than ~1.31 Å (Figure 7b), the D_0 state is characterized by an unpaired electron primarily in the $2p\pi$ orbital of NH_2, the D_1 state is characterized by an unpaired electron mainly in the $2p$ orbital of oxygen (which is part of the delocalized π -electron system), and the D_2 state is characterized by an unpaired electron mainly in the σ orbital of oxygen. At r(OH) distances longer than ~1.31 Å, the D_0 and D_1 states switch their characters. Analogous cuts through the lowest three adiabatic potential energy surfaces of the ArOH···NH_2 system for the case when the hydrogen transfers in the ring plane are shown in Figures 7c and 7d. In each case, a D_0/D_1 conical intersection has been found, with the in-plane intersection of Figure 7d about 6 kcal/mol higher than the crossing point shown in Figure 7b. Figure 8 shows analogous results for the PhOH···$OOCH_3$ system, where only the D_0 and D_1 states are considered. At r (OH) distances shorter than ~ 1.18 Å (Figure 8b), the D_0 state is characterized by an unpaired electron in the 2π orbital of $OOCH_3$, and the D_1 state is characterized by an unpaired electron in the at $2p\pi$ orbital of oxygen; the shapes of these two orbitals, 38a″ and 37a′ are illustrated in panel (b) of Figure 5. In the vicinity of a conical intersection, at r(OH) ≈ 1.18 Å, the D_0 and D_1 states switch their characters.

As it can be seen from comparing Figure 7a with 7b, and Figure 7c with 7d, the slopes of the two lowest adiabatic PESs and the locations of crossing points on the H-transfer reaction path are rather different at the CASSCF and MCQDPT levels, indicating, as expected, that dynamical correlation is essential for a quantitative description of these systems. We therefore obtain our estimates of the critical energy gaps by MCQDPT calculations (at FORS-optimized geometries for the saddle point, and the intersection points shown in Figures 7b and 8b for the conical intersection). In this way, the conical intersection for the ArOH···NH_2 system is calculated to be 0.2 kcal/mol above the ground state energy at the SP structure. In the case of ArOH···$OOCH_3$, the corresponding energy difference is only 0.05 kcal/mol.

Mechanistic Discussion in Terms of Topographical Features of the Potential Energy Surfaces. Since the saddle point is generally the shoulder of a conical intersection,[37] the intersection is to the side of the minimum-energy reaction path, not along it. Thus, we expect a local minimum in the gap between the two adiabatic states as a system moves along the minimum-energy reaction path and passes the conical intersection. If the intersection is strongly avoided (large gap) along this path, the hydrogen atom is likely to transfer electronically adiabatically with the singly occupied orbital changing its character gradually and remaining singly occupied along the whole reaction path; in such a case the reaction is expected to occur entirely on the ground potential energy surface and can be considered to be the transfer of a hydrogen atom. If the intersection is narrowly avoided (small gap), then the reaction takes place on both potential energy surfaces and the electron and proton need not transfer synchronously. Thus, although PCET is net adiabatic, it involves some nonadiabatic character in the critical region along the reaction path. These nonadiabatic events would be promoted by a small energy gap between D_0 and D_1 along the reaction path due to the conical intersection being close to the saddle point, as in the two cases studied here.

The energies of the SP and MECP structures thus serve as convenient characteristic quantities by which one can judge the likelihood of the two mechanisms. The saddle point serves as the lowest-energy point on the conventional transition state hypersurface separating reactants from products for the electronically adiabatic HAT mechanism. It also provides a first approximation for the variational transition state, and as such it may be used for quantitative estimates of effective threshold energies and adiabatic reaction rates, especially if one includes multidimensional tunneling effects. (The importance of tunneling in reaction 1 with the $^{\bullet}OOCH_3$ radical has been recently demonstrated.)[38] The minimum-energy crossing point likewise provides a reasonable starting point for estimating the probability of a nonadiabatic reaction. Its usefulness for photochemical reactions is mitigated by the circumstance that the system energy may be considerably higher than the energy of the MECP, and therefore one must consider a wide expanse of the conical intersection seam in order to include all potentially important reaction paths.[39,40] However, for thermally activated nonadiabatic reactions, such as the PCET mechanism under consider-

(37) (a) Allison, T. C.; Lynch, G. J.; Truhlar, D. G.; Gordon, M. S. *J. Phys. Chem.* **1996**, *100*, 13575. (b) Truhlar, D. G.; Mead, C. A. *Phys. Rev. A* **2003**, *68*, 32501.

(38) Navarette, M.; Rangel, C.; Espinosa-Garcia, J.; Corchado, J. C. *J. Chem. Theory Comput.* **2005**, *1*, 337.

ation here, the MECP does provide a first approximation to the effective threshold energy, if one includes two other caveats and complications: (i) the system may tunnel to the conical intersection or its neighborhood; (ii) the chance of a classical trajectory or the center of a wave packet actually passing through a conical intersection is small because it is a (3*N*-8)-dimensional seam buried in a (3*N*-6)-dimensional internal-coordinate space, and it does not form a hypersurface dividing reactants from products (in contrast to a transition-state seam, which is a dividing surface and which has dimensionality 3*N*-7). With these distinctions between these two kinds of critical points in mind, it is useful to use them to discuss the competition between the HAT and PCET mechanisms.

Geometric proximity of the SP and MECP structures in the model ArOH···R complexes shows not only that H transfer in such systems may occur nonadiabatically but also that the HAT and PCET mechanisms are not mutually exclusive categories. (The latter observation is not new, but the present framework provides a new way to understand it.) Although a trajectory or the center of a wave packet is unlikely to pass precisely through the saddle point and is even less likely to pass through the MECP, we can still use these topographical features to understand why trajectories that pass through the transition state dividing surface near the saddle point are adiabatic if there is a large gap between the adiabatic surfaces, and those that pass close to the conical intersection are nonadiabatic. When these critical points are close in geometry, all trajectories may have some nonadiabatic character, and the mechanisms blend into each other.

In the case of $ArO\cdots NH_2$, as one moves along the reaction path from the SP toward reactants, the D_0 state acquires the dominant $(29a)^2(30a)^1$ character with the unpaired electron in the nitrogen's SOMO, while the D_1 state becomes dominated by the $(29a)^1(30a)^2$ configuration with the unpaired electron in a π MO of phenol. On going down from the SP to the products, the characters of these states change in opposite directions; in particular, the ground electronic state acquires the dominant $(29a)^2(30a)^1$ character. A strong configuration mixing in the intermediate region results in an avoided state crossing and produces a D_1-D_0 energy gap of ~30 kcal/mol in the vicinity of the SP. This is smaller than usual[41] but large enough to result in an adiabatic reaction. Although the energy difference between SP and MECP structures for this system is less than 1 kcal/mol, the rather large energy gap of ~30 kcal/mol between the D_0 and D_1 states at the SP structure is due to a steep slope of the D_1 potential in the direction from the MECP toward the SP (in the absence of other complications, such as in the simplest case of the three-electron H + H_2 reaction, one would expect that the D_0 state goes down by an amount comparable to that by which the D_1 state goes up when one changes a geometry from a conical intersection to a saddle point structure). The large energy gap at the SP geometry along with a relatively small lowering in energy of the D_0 state at the SP relative to the MECP structure can be understood by considering the electronic structure of the D_0 and D_1 states and the molecular geometries of the SP and MECP structures. At the SP, the D_0 state is the one with the unpaired electron in a π orbital of the phenoxyl ring, whose geometry is rather similar to the geometry at the MECP, which is why the energy of this state is not significantly different from its energy at the MECP. In contrast, the D_1 state is dominated by a configuration with the unpaired electron in the lone pair orbital of the NH_2 radical, whose geometry is rather different at the SP as compared to the MECP (see, e.g., panel c of Figure 5) as a consequence of sp^3-hybridization (recall that the radical center in the ground electronic state of the NH_2 radical is sp^2-hybridized), which is why the energy of this state is considerably higher than its energy at the MECP. The energetic proximity of the SP and MECP structures indicates that both electronically adiabatic and nonadiabatic reaction pathways can be accessible, the former via the region with a large energy gap between the D_0 and D_1 states and the latter via the region with a small gap.

Even when the reaction path does not pass near the conical intersection and even if the reaction mechanism is best described as an HAT type of reaction, one may analyze the reaction in terms of the relative percentages of the configurationally uniform diabatic states corresponding to reactants and products. It has been noted that "the transition state of the majority of chemical reactions has the potential for being unbalanced.[43] This has been attributed to the involvement of two or more processes such as bond breaking, bond formation, or electron delocalization.[43] While such effects have been widely analyzed[43] in terms of linear free energy relationships,[44,45] progress in understanding the root causes of nonsynchronicity has lagged. Since a diabatic crossing of electronic states leads to a change in the dominant character of the ground-state electronic wave function, a diabatic energy gap reaction coordinate may be defined (by analogy to the Marcus theory of weak-overlap electron transfer) as

$$w = E_1 - E_2 \tag{2}$$

where E_1 is the energy of the diabatic state with the electron on the donor, and E_2 is the energy of the diabatic state with the electron on the acceptor. Then the location where w increases through zero may be considered to be the halfway point of the transfer of the electron. Similarly, the halfway point of the transfer of a proton can be defined as the place where an appropriately defined geometric reaction coordinate passes through zero; for example one can define the geometric reaction coordinate as

$$z = r_{D-H} - r^R_{D-H} - \left(r_{A-H} - r^P_{A-H}\right) \tag{3}$$

where A is the acceptor atom (N in $^{\bullet}NH_2$ or O in $^{\bullet}OOCH_3$), D is the donor atom (O of $PhO^{\bullet}$), r_{X-H} is the distance from X to the transferring H, and superscripts R and P denote values at reactants and products, respectively. With these definitions, the discussion above shows one possible way to understand the electronic origin of nonsynchronicity, namely, diabatic sequentiality, by which a diabatic curve crossing occurs before, concurrent with, or after the midpoint of a nuclear-coordinate displacement variable. An example, corresponding to electron

(39) (a) Migani, A.; Sinicropi, A.; Ferre, N.; Cembran, A.; Garavelli, M.; Olivucci, M. *Faraday Discuss.* **2004**, *127*, 129. (b) Toniolo, A.; Olsen, S.; Manohar, L.; Martinez, T. J. *Faraday Discuss.* **2004**, *127*, 149.
(40) Truhlar, D. G. *Faraday Discuss.* **2004**, *127*, 242.
(41) In most hydrogen transfer systems, especially in those that have only σ bonds and no π bonds, the energy gap that separates the electronic ground and the first excited state at the saddle point geometry is expected to be significantly larger. As a prototype case, one can consider the hydrogen transfer in the H + H_2 system, where the D_1-D_0 energy separation at the saddle geometry is greater than 5 eV.[42]
(42) Porter, R. N.; Stevens, R. M.; Karplus, M. *J. Chem. Phys.* **1968**, *49*, 5163.
(43) Bernasconi, C. F. *Adv. Phys. Org. Chem.* **1992**, *27*, 119.
(44) Lewis, E. S. In *Investigation of Rates and Mechanisms of Reactions*, 4th ed.; Bernasconi, C. F., Ed.; Techniques of Chemistry Series 6; John Wiley & Sons: New York; Part I, p 871.
(45) Grunwald, E. *Thermodynamics of Molecular Species*; Wiley: New York, 1997; p 94.

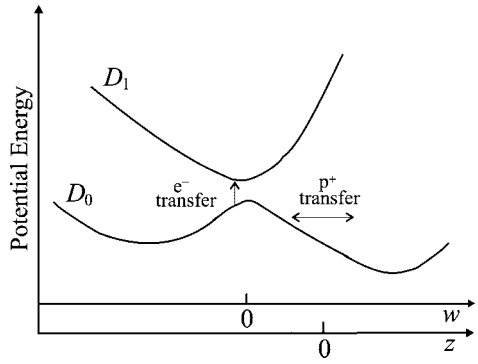

Figure 9. Schematic electronically adiabatic potential energy curves along a hydrogen transfer coordinate showing how the location of the avoided crossing (corresponding to a nearby conical intersection) controls the character of proton-coupled electron transfer. The tick mark at $w = 0$ shows the origin of the diabatic reaction coordinate defined in 2, and the tick mark at $z = 0$ shows the origin of the geometric reaction coordinate defined by 3. The conical intersection is to the side of the saddle point. To the left of $w = 0$, the lower adiabat D_0 corresponds to the electron quasilocalized on the donor, and D_1 corresponds to the electron quasilocalized on the acceptor; to the right of $w = 0$, the diabatic characters of the two adiabats are switched. The vertical arrow corresponds to a Franck–Condon transition from the electron being quasilocalized on the donor to it being quasilocalized on the acceptor.

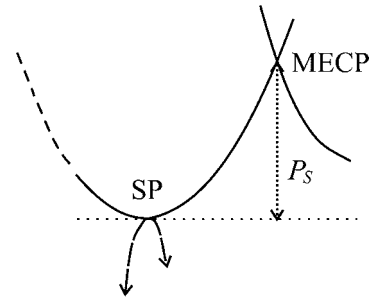

Figure 10. This figure illustrates the specific prominence (P_S) of the energy-minimized structure of a conical intersection of the two states as the energy of this structure relative the saddle point structure that arises as result of an avoided crossing of these states.

transfer preceding proton transfer, is shown in Figure 9. Clearly this explanation will be most useful when the electronic character shifts in a localized regime. This could be promoted by a small resonance interaction between the diabatic states, which could occur because of globally valid considerations involving the natures of the orbitals involved or because the saddle point happens to be close to a conical intersection, a situation which can be promoted by a low-energy conical intersection, as in reaction 1.

In Figure 9, we drew the electron transfer as a vertical line. Since the abscissa is a function of nuclear coordinates, a vertical line corresponds to a Franck–Condon transition in coordinate space, which is a realistic model. Since the lower state corresponds to an untransferred electron, and the upper state, to a transferred one, this vertical line corresponds to a transfer of the electron from a diabatic state on the donor to a diabatic state on the acceptor. But this is just one way to treat the event. In an exact treatment of dynamics the results are independent of representation. Thus one may view the electron transfer as a state change from a localized diabatic state on the donor to a localized diabatic state on the acceptor, or one may treat the transition in terms of adiabatic states.

From a very general perspective, most saddle points may be viewed as shoulders of conical intersections.[37] (In contrast, cases when a conical intersection occurs along the minimum-energy path, before or after the saddle point, should be encountered much less frequently and in particular only when there is a third diabatic state involved,[46] not just the two states that give rise to the avoided crossing at the saddle point.) The shoulder analogy provides a conceptual framework for understanding the question raised above of whether there is a small energy gap along the reaction coordinate when one passes the conical intersection. The difference in the Born–Oppenheimer energies of the reaction saddle point and the closest point on a conical intersection is in some respects analogous to the topographic "prominence", which is the height of a mountain peak above the highest saddle point connecting it to another peak, although the analogy is not perfect because a "peak" in this case is actually a (3*N*-8)-dimensional seam and because we are not concerned whether the peak on the other side of the saddle is higher. We will label this kind of prominence associated with a specific saddle point as specific prominence. This is shown schematically in Figure 10. For a thermally activated reaction, such as reaction 1, the low specific prominence of a conical intersection would indicate its importance for reaction dynamics. Usually the minimum-energy conical intersection is much higher in energy than the saddle point, as in the H + H_2 reaction,[47a] where the MECP is at 63 kcal/mol and the SP is at 10 kcal/mol, both relative to reactants. Occasionally, the difference is very small, as in the $O(^3P)$ + CH_4 reaction, where, at one level of calculation,[47b] the SP is at 17.8 kcal/mol relative to reactants and a Jahn–Teller MECP is very close in geometry and is higher by less than 0.1 kcal/mol. (A different kind of example of a close energetic proximity of two electronic states near the transition state in a Jahn–Teller system is a hole transfer reaction in bismethyleneadamantane.[47c,d]) In general the semiglobal representations of a saddle point in close proximity to a conical intersection require an expansion through at least quadratic terms in a geometric deviation from the conical intersection.[48] Although we do not pursue such analytic models here, they would be a fruitful area for future investigation. We do, however, show how the recognition that the saddle point is the shoulder of a conical intersection leads to a unified perspective on the two mechanisms; we present further elaboration of this perspective in the next paragraph.

One of the most widely used representations of continuously shifting reaction mechanisms is provided by the More O'Ferrall–Jencks diagram.[49–51] For 1,2-elimination reactions, this has the E1 mechanism proceeding through one corner, E1cb proceeding through another, and the E2 mechanism corresponding to synchronous proton transfer and leaving group departure is

(46) An example is given by Figure 7c and 7d. The D_0/D_1 interaction is associated with a conical intresection of the states responsible for the saddle point, and it is strongest near the saddle point, whereas the D_1/D_2 interaction involves a third state and is strongest at a position after the saddle point.

(47) (a) Varandas, A. J. C.; Brown, E. F.; Mead, C. A.; Truhlar, D. G.; Blais, N. C. *J. Chem. Phys.* **1987**, *86*, 6258. (b) Corchado, J. C.; Espinosa-Garcia, J.; Roberto-Neto, O.; Chuang, Y. Y.; Truhlar, D. G. *J. Phys. Chem. A* **1998**, *102*, 4899. (c) Blancafort, L.; Jolibois, F.; Olivucci, M.; Robb, A. *J. Am. Chem. Soc.* **2001**, *123*, 722. (d) For a recent review see: Carpenter, B. K. *Chem. Soc. Rev.* **2006**, *35*, 736.

(48) (a) Thompson, T. C.; Truhlar, D. G.; Mead, C. A. *J. Chem. Phys.* **1985**, *82*, 2392. (b) Köppel, H. *Faraday Discuss* **2004**, *127*, 35. (c) Blancafort, L.; Bearpark, M. J.; Robb, M. A. *J. Phys. Chem. A* **2007**, *111*, 2182.

represented as a diagonal line.[49] For nucleophilic substitution reactions, the More O'Ferrall–Jencks diagram has S_N1 reactions proceeding through one corner, two-step addition–elimination reactions proceeding through another corner, and concerted S_N2 reactions corresponding to a diagonal.[52] Similar analyses have been applied to proton[43] and hydride transfer reactions.[53] In all four of these cases, the axes correspond to bond breaking and to bond formation, so that the plot refers only to nuclear coordinates, not to the nature of the electronic wave function. However, to generalize this kind of analysis to describe the HAT-PCET continuum, we put, following Mayer,[5b] the electron transfer character of the wave function on one axis and the hydrogen nuclear coordinate on the other axis, as in each horizontal slice of panel e of Figure 11. Furthermore, we generalize the plot to dynamical bottlenecks that result not only from barriers on the ground-state potential energy surface but also from the properties of seams of conical intersections. As a result, each position in this diagram indicates the proton coordinate and the electron character of a possible ensemble-average dynamical bottleneck for a PCET or an HAT reaction (or a reaction following an intermediate mechanism with some of both characters). Deviations from the diagonal route indicate the degree of nonsynchronicity. The vertical axis, which is the energy gap between the two adiabatic states at the reaction saddle point, indicates nonadiabaticity. Four different cases with large and small energy gaps at the saddle point when the latter is close or far from the conical intersection are schematically illustrated in panels a–d of this figure. The abscissa for the plots in panels a–d is the distance along a path, transverse to the reaction coordinate, that connects a point on the conical intersection seam to the saddle point. In the upper slice of the diagram in panel e, the areas next to the corners are shaded to indicate the smaller probability for a mechanism with a significant degree of nonsynchronicity as the gap becomes large. The locations of nonsynchronous cases *a*, *b*, *c*, and *d* are marked on the slice of the 3D PCET/HAT mechanistic diagram of panel e. Panel e also shows the locations of mechanisms *a*′, *b*′, *c*′, and *d*′. One cannot see the difference between mechanistic cases *a* and *a*′ (or *b* and *b*′, etc.) in panels a–d of Figure 11, but this difference can be understood by plots like that in Figure 9 which shows potentials along the minimum energy path through the saddle point. Figure 9 shows the case *c*′ where electron transfer precedes proton transfer, but one could draw similar diagrams for other cases. Although points in Figure 11e correspond to dynamical bottlenecks of various reactions, and curves in Figure 11e correspond to sequences of such bottlenecks for sets of reactions, we can place Figures 9 and 11 in a unified perspective by considering reaction paths through the same coordinate system as used in Figure 11e. Then we could replace *z* in Figure 9 by the distance, calling it *s*, along a reaction path that goes from the lower left to the upper right in either of the horizontal slices of Figure 11e, whereas the coordinate *d* in panels a–d of Figure 11 measures the distance along a path (transverse to the reaction path) that connects the saddle point to a point on the conical intersection seam.

The present case, illustrated schematically in Figure 6, is particularly interesting for three reasons. First, the low specific prominence of the conical intersection is not required by state symmetry (although, as discussed above, it can be understood in terms of orbital symmetry). Second, the geometric and energetic proximity of the MECP to the SP can be modulated in gas-phase ArOH + RH reactions by changing the nature of the arene ring or its substituents or by varying R (here we considered only R = $^{\bullet}NH_2$ and R = $^{\bullet}OOCH_3$). (For example, it is expected that the electron-donor substituents in the phenol ring will lower relative energies of both SP and MECP structures due the lowering of the D_1 state that arises from an excitation of an electron from the phenol π orbital. Numerous studies that consider correlations between rate constants of reaction 1 and substituent effects are reported elsewhere.)[54] Third, in an enzyme and liquid solvent environment, the properties of the MECP and SP can also be modulated by noncovalent effects, including electrostatic polarization.

An advantage of interpreting chemical reactivity in terms of diabatic states is that one can gain insight into the controlling orbitals from electronic spectroscopy and photodissociation.[55] Recall that, in an isolated phenol molecule, the ground electronic state (S_0) is diabatically correlated to the first excited ($^2\sigma$) state of the phenoxyl radical, whose ground electronic state ($^2\pi$) is diabatically correlated to an excited (S_2) state of the phenol molecule, and a conical intersection of the two states can be accessed by OH stretching in the planar geometry.[56] A similar picture for the PhO···NH_2 system is shown in Figure 7c and 7d. In particular, the lowest electronic state in the product region of the ArO···NH_3 system that corresponds to the $^2\pi$ state of the phenoxyl radical is diabatically correlated to the D_2 state of the ArOH···NH_2 complex and exhibits a conical intersection with the state that corresponds to the $^2\sigma$ state of the phenoxyl radical in the product region. This indicates that a portion of the D_0/D_1 conical intersection in ArOH···R complexes in the ring plane is related to the $^2\sigma/^2\pi$ conical intersection in the prototype phenol molecule and that it represents a persistent factor to be considered for H-atom abstractions from phenol.

Other Viewpoints. We have shown how electronic nonadiabaticity provides a unified view of HAT and PCET in terms of topographic features of the potential energy surfaces and coupling of the two diabatic states that correspond to ground electronic state reactants and ground electronic state products. But this is not the only criterion that has been used to classify

(49) More O'Ferrall, R. A. *J. Chem. Soc. B* **1970**, 274.
(50) Jencks, W. P. *J. Chem. Rev.* **1972**, *72*, 705.
(51) Jencks, W. P. *J. Chem. Rev.* **1985**, *85*, 511.
(52) (a) Albery, W. J.; Kreevoy, M. M. *Adv. Phys. Org. Chem.* **1978**, *16*, 87. (b) Kreevoyi, M. M.; Truhlar, D. G. In *Investigation of Rates and Mechanisms of Reactions*, 4th ed.; Bernasconi, C. F., Ed.; Techniques of Chemistry Series 6; John Wiley and Sons: New York; Part I, p 13.
(53) (a) Kreevoy, M. M.; Lee, I.-S. *J. Am. Chem. Soc.* **1984**, *106*, 2550. (b) Harris, J. M.; Shafer, S. G.; Moffatt, J. R.; Becker, A. R. *J. Am. Chem. Soc.* **1929**, *101*, 3295.
(54) (a) Burton, G. W.; Ingold, K. U. *J. Am. Chem. Soc.* **1981**, *103*, 6472. (b) Doba, T.; Burton, G. W.; Ingold, K. U. *J. Am. Chem. Soc.* **1983**, *105*, 6505. (c) Gilchrist, J.; le, G.; Burton, G. W.; Ingold, K. U. *Chem. Phys.* **1985**, *95*, 473. (d) Burton, G. W.; Doba, T.; Gabe, E. J.; Hughes, L.; Lee, F. L.; Prasad, L.; Ingold, K. U. *J. Am. Chem. Soc.* **1985**, *107*, 7053. (e) Lucarini, M.; Pedulli, G. F.; Cipollone, M. *J. Org. Chem.* **1994**, *59*, 5063. (f) Brinck, T.; Haeberlein, M.; Jonsson, M. *J. Am. Chem. Soc.* **1997**, *119*, 4239. 1997, 119, 4245. (g) Wright, J. S.; Carpenter, D. J.; McKay, D. J.; Ingold, K. U. *J. Am. Chem. Soc.* **1997**, *119*, 4245. (h) Wright, J. S.; Johnson, E. R.; DiLabio, G. A. *J. Am. Chem. Soc.* **2001**, *123*, 1173. (i) Katarina, N. M. *J. Mol. Struct. THEOCHEM* **2007**, *818*, 141.
(55) (a) McDonald, J. D.; LeBreton, P. R.; Lee, Y. T.; Herschbach, D. R. *J. Chem. Phys.* **1972**, *56*, 769. (b) Truhlar, D. G.; Dixon, D. A. In *Atom-Molecule Collisions Theory*; Bernstein, R. B., Ed.; Plenum: New York, 1979; p 595.
(56) (a) Sobolewski, A. L.; Domcke, W.; Dedonder-Lardeux, C.; Jouvet, C. *Phys. Chem. Chem. Phys.* **2002**, *4*, 1093. (b) Abe, M.; Ohtsuki, Y.; Fujimura, Y.; Lan, Z.; Domcke, W. *J. Chem. Phys.* **2006**, *124*, 224316.

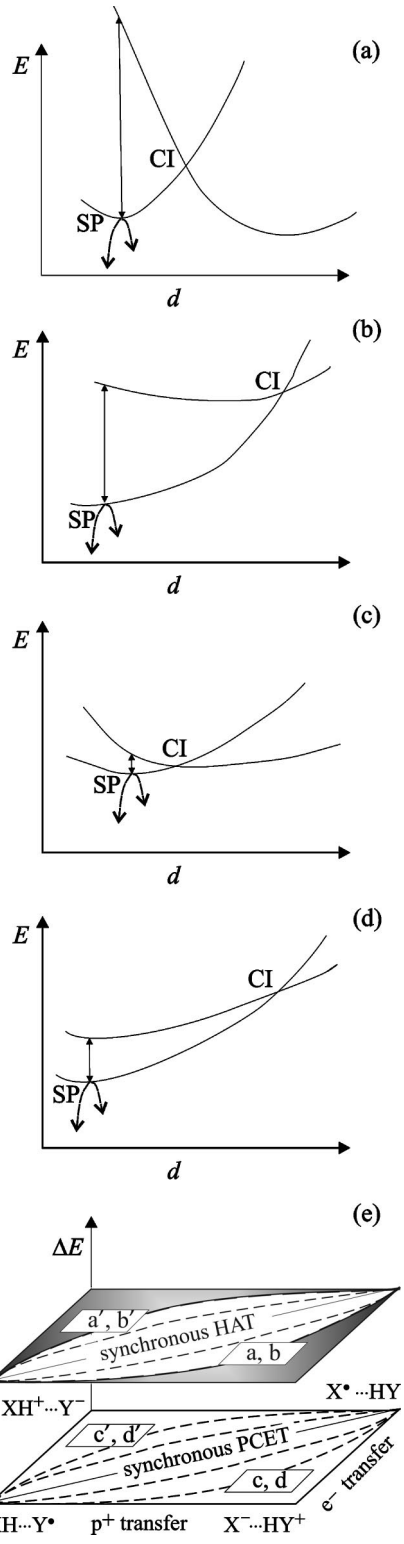

Figure 11. (a) Upper and lower adiabatic points as functions of the distance d from a point on the conical intersection seam to the saddle point for mechanistic cases a and a'. (b) Same for cases b and b'. (c) Same for cases c and c'. (d) Same for cases d and d'. (e) Generalized More O'Ferrall−Jencks diagram for the HAT-PCET continuum. The edge routes from reactant (lower left) to product (upper right) correspond to a sequence of ensemble-averaged dynamical bottlenecks for a stepwise mechanism, and the dashed routes correspond to sequences of ensemble-averaged dynamical bottlenecks for concerted processes with various amounts of nonsynchronicity and transition state imbalance. The vertical axis is the energy gap between the two lowest adiabatic states at the reaction saddle point.

reactions as HAT or PCET. Another criterion that may be useful is synchronicity, but this is difficult to apply because almost all reactions involve multiple elements (e.g., changes in bond lengths and changes in hybridization states) that are not precisely synchronous. Somewhat more satisfactory is to call a reaction PCET when the proton and electron are transferred from different sites in the molecule or are transferred to two separate reagents[5b] or when outer-sphere electron transfer is concerted with deprotonation by another reagent.[5b] One might attempt to generalize this to the cases when the electron and proton are transferred to different regions of the same molecule, but this clearly leads to ambiguity since the polarity of the products usually differs from that of reagents and the precise "location" of the transferred electron is ambiguous. Note that all these criteria focus exclusively on the ground-state potential energy surface and charge distribution.

One may also use orbital-based criteria. Consider again the general reaction 1. When R is an oxygen-centered π-radical, reaction 1 has long been known to have a low activation energy and an unusually small Arrhenius preexponential factor (e.g., as compared to the known data for hydrogen atom abstraction from C−H bonds)[57] if one or both oxygens are sterically hindered.[18] This behavior has been attributed, with the help of density functional theory calculations, to the PCET mechanism in O−H···O systems as opposed to the HAT mechanism in C−H···C systems.[19] In particular, it has been found[19] that the degenerate hydrogen atom transfer in the phenol/phenoxyl radical system involves a transfer of a proton and electron between two different sets of molecular orbitals, while a similar reaction in the toluene/benzyl radical system is characterized by a transfer of a proton and an electron between the same set of molecular orbitals; this explanation of the differences between the HAT and PCET mechanisms in terms of the molecular orbitals that accept the electron and the proton has been generalized for an arbitrary X−H···Y → X···H−Y reaction.[58] Because only the ground state is considered, there is no prediction as to the extent of electronic nonadiabaticity.

A different perspective on the fundamental differences of these two type of reactions in terms of electronic nonadiabaticity was proposed recently by Skone et al.[11] They considered both diabatic and adiabatic representations, and they noted that even when the reaction is overall electronically adiabatic, it can be locally electronically nonadiabatic in the interaction region. We have also pointed this out in the present analysis. Skone et al. further pointed out that the phenoxyl/phenol reaction in which the electron and proton were previously identified[19] as transferring between different orbitals is locally electronically nonadiabatic, while the benzyl/toluene reaction, which was previously identified[19] as being dominated by orbitals oriented along the donor–acceptor axis, is electronically adiabatic. Skone et al. conclude that electronic nonadiabaticity is a diagnostic for distinguishing HAT from PCET with the former being locally electronically adiabatic. The present study is consistent with the conclusions of Skone et al. and provides further support for the role of electronic nonadiabaticity. In addition, we analyze the topographic features of the coupled potential energy surfaces that underlie electronic nonadiabaticity and use them to illustrate the relation and connectivity between the HAT and PCET mechanisms in both the adiabatic and diabatic representations.

(57) Benson, S. W. *Thermochemical Kinetics*, 2nd ed.; Wiley Interscience: New York, 1976; p 156.
(58) Lingwood, M.; Hammond, J. R.; Hrovat, D. A.; Mayer, J. M.; Borden, W. T. *J. Chem. Theory Comput.* **2006**, *2*, 740.

We can compare the orbital-based approach[19] to the present diabatic-state approach for the reactions $ArCH_2 + ArCH_3 \rightarrow ArCH_3 + ArCH_2$ and $ArO + ArOH \rightarrow ArOH + ArO$. In the orbital-based classification, the former (benzyl) case is HAT because the electron transfers into the SOMO that becomes the new C−H bonding orbital in the product, whereas the latter (phenoxy) case is PCET because the electron transfers into a different orbital from the one that becomes a bonding orbital for the transferred H.[19] The classification is enabled by the fact that the saddle point is only slightly lower than a similar planar geometry where symmetry can be used to classify the orbitals; it is harder or impossible to use this argument in unsymmetric cases.

In contrast, the topographical considerations emphasized in the present article give a different view of these cases. The benzyl case is HAT because of a high prominence, and the phenoxy case is either PCET or a mixture of PCET and HAT because of a much lower prominence. Since the argument[37] that saddle points are the shoulders of conical intersections is not limited to cases with symmetry elements, this kind of adiabatic viewpoint is very general and broadly applicable.

4. Summarizing Remarks

This paper shows how the HAT and PCET mechanisms can merge in $XH\cdots Y^{\bullet}$ systems and presents a framework for understanding this phenomenon in terms of topographic features of the Born–Oppenheimer potential energy surfaces, in particular saddle points and conical intersection seams. This framework is illustrated by the results of electronic structure calculations on two model reactions between phenol and the free radicals NH_2 and $OOCH_3$. A PCET mechanism involves the coupled potential energy surfaces in the vicinity of a conical intersection of the D_0 and D_1 states, whereas an HAT mechanism corresponds to an adiabatic reaction occurring entirely on the ground electronic state PES, via a dynamical bottleneck that results from an avoided crossing of these states. A unified perspective on these mechanisms is provided by recognizing that the reaction saddle point is to the side of the intersection seam and is located on a shoulder of this intersection. Energetic accessibilities of saddle points and low-lying portions of the intersection seam, along with the topographic prominence (defined as the difference in the Born–Oppenheimer energies of a saddle point and the nearest point on the intersection seam), are characteristic features that determine the likelihood of the PCET and HAT mechanisms. The reactions studied above illustrate the case of a small topographic prominence (at most a few kcal/mol). The results suggest that in such systems, the D_0/D_1 conical intersection is a determinative element in the mechanistic competition between and possible blending of H transfer and proton-coupled electron transfer.

A related concept that provides further unity to the perspective is the concept of diabatic states. We associate the reactant of the HAT/PCET reaction with one molecular mechanics structure and the product with another. Each molecular mechanics structure is identified with a valence bond wave function, and the valence-bond wave functions are zero-order approximations to the diabatic states; the essential characteristic of diabatic state wave functions is that they preserve their electronic structural character throughout a reaction. The saddle point governing HAT corresponds to an avoided crossing of the two adiabatic states that approximately span the same space as these diabatic states,[59] and the conical intersection governing PCET corresponds to the crossing, at a higher energy, of the same two diabatic states at a place where their coupling vanishes. The diabatic states also cross near the saddle point, but their coupling does not vanish there. Thus, the conical intersection of the lowest two adiabatic states corresponds to the subseam of the diabatic crossing seam where the diabatic coupling vanishes, whereas the saddle point on the lowest adiabatic potential energy surface is one point near the portion of the diabatic crossing seam where the diabatic coupling does not vanish.

We also compared our approach in terms of the geometry (topography) of potential energy surfaces to previous work where the mechanistic distinction between the HAT and PCET mechanisms has been made in terms of participating molecular orbitals (refs 19, 58, and references therein), based on whether a proton and an electron are transferred between the same or different sets of molecular orbitals. In fact, in an arbitrary $XH\cdots Y^{\bullet}$ reaction, the D_0/D_1 intersection seams and the saddle points on the shoulders of these seams represent inherent features of the lowest energy potential surfaces, independent of whether the same or different orbitals are involved, and as a consequence, the competition between HAT and PCET mechanisms is understood in terms of the energetic accessibility of saddle points and intersection seams that are connected by a ridge and have the same underlying diabatic states. This provides a framework to understand the dependence on the molecular structure of reactants, steric constraints, and the environment.

More generally, consideration of the diabatic sequentiality involved in the PCET mechanism provides a way to understand the transition state imbalance in hydrogen transfer reactions that are not completely synchronous.

Acknowledgment. This work was supported in part by the National Science Foundation under Grant No. CHE07-04974, and it was carried out within the framework of a research project financed by the Fund for Scientific Research (FWO-Vlaanderen). The support of the KU Leuven Research Council (GOA program) is gratefully acknowledged.

Supporting Information Available: Full details of the computational methods, optimized molecular geometries in Cartesian coordinates, tables with geometrical parameters in internal coordinates, and shapes of active molecular orbitals. This material is available free of charge via the Internet at http://pubs.acs.org.

JA7102907

(59) (a) London, F. Z. *Elektrochem.* **1929**, *35*, 552. (b) Hirschfelder, J. O.; Eyring, H.; Rosen, N. *J. Chem. Phys.* **1936**, *4*, 121. (c) Yasumori, I. *Bull. Chem. Soc. Jpn.* **1959**, *32*, 1110. (d) Porter, R. N.; Karplus, M. *J. Chem. Phys.* **1964**, *40*, 1105. (e) Shaik, S.; Shurki, A. *Angew. Chem., Int. Ed.* **1999**, *38*, 586.